

INVESTIGATION OF A TRANSONIC AXISYMMETRIC BACKWARD-FACING STEP FLOW BY MEANS OF HIGH RESOLUTION PIV

Sven Scharnowski, Christian J. Kähler

Institute of Fluidmechanics and Aerodynamics
Bundeswehr University Munich
85577 Neubiberg, Germany
sven.scharnowski@unibw.de

ABSTRACT

This work analyzes the axisymmetric backward-facing step flow at a Mach number of 0.7 and a Reynolds number of 10^6 , based on the forebody's diameter, in order to achieve fundamental understanding of the separating and reattaching flow and to generate a data basis for the validation of numerical flow simulations. Due to the strong progress of optical flow measurements in the last years it was possible for the first time to resolve all flow scales down to $180\ \mu\text{m}$ ($\approx 1\%$ of the step height) with high precision. A large ensemble, consisting of 21 500 statistically independent PIV image pairs, allows for the reliable and accurate estimation of the mean velocity distribution as well as of the Reynolds shear stress distribution on the plane of symmetry. It was found that the ensemble-averaged flow reattaches 1.06 times the fore body's diameter downstream of the point of separation on the models rear sting. In the corner of the primary recirculation region a secondary vortex with opposite mean circulation direction is generated on average. The Reynolds shear stress distribution shows high intensity within the developing shear layer as well as at the centre of the primary recirculation region and develops a broad maximum at an axial location around the reattachment location. The shear stress in the separated region was found to be strongly influenced by small scale turbulent structures.

INTRODUCTION

The backward-facing step flow was extensively studied experimentally and numerically (Eaton & Johnston, 1981; Bradshaw & Wong, 1972). The geometry is rather simple the flow field however, is relatively complex, as illustrated in figure 1. The incoming turbulent boundary layer developing along the forebody is forced to separate at the sharp edge. As a result of a Kelvin-Helmholtz instability tiny coherent vortices are generated in the first part of the very thin shear layer. The vortices grow in size and strength while travelling downstream. This causes, on average, a broadening of the shear layer with increasing distance from the point of separation and an amplification of the turbulent fluctuations within this region. Due to the enhanced turbulent mixing the shear layer reattaches on the sting. The mean flow field is characterized by a large recirculation region, which is separated from the outer region by the dividing streamline. The reattachment location is not fixed in space and time due to the dynamic of coherent vortices. Some of the coherent shear layer vortices

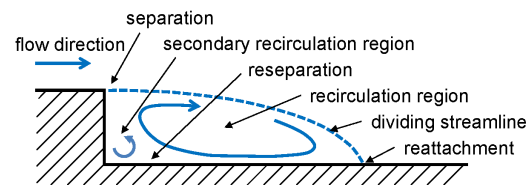


Figure 1: Backward-facing step flow field.

move into the recirculation region, according to Chandrasuda (1975) and McGuinness (1978) and they interact with the next generation of shear layer vortices, if they survive sufficiently long before they vanish due to viscosity. Due to this feedback, the shear layer of a backward-facing step differs significantly from a free shear layer. Furthermore, the vortices travelling upstream into the primary recirculation region decay into smaller vortices due to secondary Kelvin-Helmholtz instabilities, or they become larger and weaker due to viscosity effects. Due to the increasing pressure with decreasing distance from the step, the upward motion of the fluid along the sting separates again. As a result, a secondary recirculation region is formed on average in the corner of the primary recirculation region with opposite sign of vorticity.

Bradshaw & Wong (1972) as well as Eaton & Johnston (1981) showed in their review papers, that for two-dimensional flows around a backward-facing step the stream-wise extension of the primary recirculation region mainly depends on the step height and on the state of the incoming boundary layer. The reattachment length is between 5 and 7 times the step height for a fully turbulent incoming flow state at the point of separation. This holds for a Reynolds number range of $Re_h = 3000 - 300000$, based on the step height. Eaton & Johnston (1981) found that the first part of the separated shear layer is similar to a plane mixing layer, since the dividing streamline is only slightly curved and the shear layer is sufficiently thin to be unaffected by the wall. The second half of the separated flow region is characterized by a strongly curved shear layer, indicated by the dividing streamline in figure 1. In this region the shear layer broadens and the Reynolds stresses increase due to the aforementioned effects. Eaton & Johnston (1981) compared several experiments on two-dimensional models and concluded that the stream-wise location with maximum stream-wise Reynolds stress and Reynolds shear

stress is close to the reattachment location or slightly upstream. Whether or not the stresses in the shear layer are even higher could not be answered so far due to the limited spatial resolution of the measurement techniques applicable to these kind of flows.

The early measurements presented in Bradshaw & Wong (1972) and in Eaton & Johnston (1981) were performed by point-like probes (LDA and hot-wire). Thus, they reveal only profiles rather than spatial distributions of the velocity and they are not able to detect instantaneous flow structures. The technical problem associated with intrusive point-wise sensors, like hot-wire and Pitot probes, is the fact that they disturb the flow of interest. Therefore, optical sensors like the Laser Doppler Anemometer (LDA) are in principle better suited because they are non-intrusive. However, all point-wise sensors have the disadvantage that they must be traversed in order to determine the global nature of the flow. This causes long measurement times and requires extremely stable flow facilities and measurement equipment. However, due to temperature changes of the flow, probe vibration, uncertainty of the traversing system, ... this is difficult to achieve in general. PIV, on the other hand, allows to measure non-intrusively thousands of two- or three-dimensional velocity fields within a few seconds and without any traversing. Furthermore, vibrations of the model or the measurement system can usually be compensated with image precessing techniques Cierpka *et al.* (2013).

This work presents planar PIV measurements of an axisymmetric generic space launcher model's wake. A large data set, acquired at a free stream Mach number of 0.7 and a Reynolds number of 1.02×10^6 (based on the model's main diameter), was evaluated (1) to compare the observations of others achieved with different measurement techniques, (2) to achieve a deep understanding of the flow physics in the axisymmetric separating and reattaching flow and (3) to create a data basis that can serve as reference for the validation of new numerical methods. The Mach number of 0.7 was selected since the mechanical loads for the main engine's nozzle in the case of a real space launcher, like ARIANE 5, are strongest in the transonic regime from $Ma \approx 0.7$ to 1.3.

MEASUREMENT SETUP

The measurements were performed in the Trisonic Wind tunnel at the Bundeswehr University in Munich (TWM). The model consists of a 36° cone with a spherical nose of $R = 5$ mm, a cylindrical forebody with a length of 164.3 mm and a diameter of $d = 54$ mm and a rear sting (21.5 mm in diameter) in the base of the cylinder, which was used for mounting the model in the test section of the wind tunnel (for details see Bitter *et al.* (2011)). For the PIV measurements the flow was seeded with DEHS tracer particles with a mean diameter of $1 \mu\text{m}$, as described in Kähler *et al.* (2002). Due to the limited run time of the facility and the large number of recordings required for reliable data evaluation, a high-repetition rate PIV system, consisting of a Quantronix Darwin Duo Nd:YLF double-pulse laser with a wavelength of 527 nm, a pulse length of $t_p \approx 120$ ns, and a pulse energy of 11 mJ per cavity at 2 kHz, was used. The illuminates particles were recorded by using a Phantom V12 high repetition rate CMOS camera (by Vision Research Inc). The recording rate was adjusted to 2000 image pairs per second. Since the vortex shedding frequency is around 900 Hz (Bitter *et al.*, 2012), the images

Table 1: Overview of the measurement parameters.

| Quantity | | Value |
|-------------------|-----------------|-------------------|
| Mach number | Ma | 0.7 |
| Reynolds number | Re_d | $1.02 \cdot 10^6$ |
| Total pressure | p_t | 1.5 bar |
| Total temperature | T_∞ | 264 K |
| Model diameter | d | 54 mm |
| Step height | $0.301 \cdot d$ | 16.25 mm |

are considered as uncorrelated, which is essential for the computation of statistical values. A total number of 21 500 PIV image pairs was acquired in four wind tunnel runs. The recorded images are $1,280 \times 400$ px in size, corresponding to a field of view of $(1.75 \times 0.5) \cdot d^2$. The Mach number was set to $Ma = 0.7$ and the Reynolds number to $Re_d = 10^6$ (related to the diameter $d = 54$ mm). The most relevant measurement parameters are summarized in Tab.1.

MEAN VELOCITY FIELD

Figure 2a shows the mean velocity field computed from 21 500 PIV image pairs using single-pixel ensemble-correlation (Westerweel *et al.*, 2004; Kähler *et al.*, 2006). According to the findings of Kähler *et al.* (2012), the spatial resolution of the vector field is $180 \mu\text{m} = 0.003d$. The main flow direction is from left to right, parallel to the x -axis. Entering the field of view from the left side at $x/d = -0.25$, the mean flow features a fully developed turbulent boundary layer state. At $x/d = 0$ the axisymmetric backward facing step causes a strong flow separation: Thereafter a thin shear layer is formed at the end of the cylindrical forebody, which broadens further downstream. At $x/d = 1.06 \pm 0.03$ the ensemble-averaged flow reattaches on the rear sting. The stream-wise extension of the recirculation region corresponds to 3.52 times the step height, which is slightly shorter than numerical predictions presented by Deck & Thorigny (2007). The difference might be due to differences in the turbulence level of the boundary layer flow along the model. Inside the dividing streamline a distinct recirculation region develops, wherein the maximum mean upstream velocity is $\approx 82 \text{ ms}^{-1}$.

The streamlines of the mean wake flow in figure 2a do not form closed loops but they bend inwards. This indicates a small out-of-plane motion within the recirculation region with a fluid drain centred at $x/d \approx 0.51$ and $y/d \approx 0.37$. Although the images are only 1280×400 px in size, the single-pixel ensemble-correlation allows for the resolution of a secondary vortex in the wake's corner, which is only $\approx 50 \text{ px} = 0.08d$ in diameter. The dividing streamline between the primary and secondary recirculation regions starts on the rear sting at $x/d \approx 0.3$ to re-separate and impinges on the base of the cylindrical main body at $y/d \approx 0.28$. The stream lines of the secondary vortex bend outwards, indicating a fluid source for the mean motion centred at $x/d \approx 0.05$ and $y/d \approx 0.23$. In order to clearly see the strong spatial changes of the mean velocity distribution from figure 2a, figures 2b to 2f show charac-

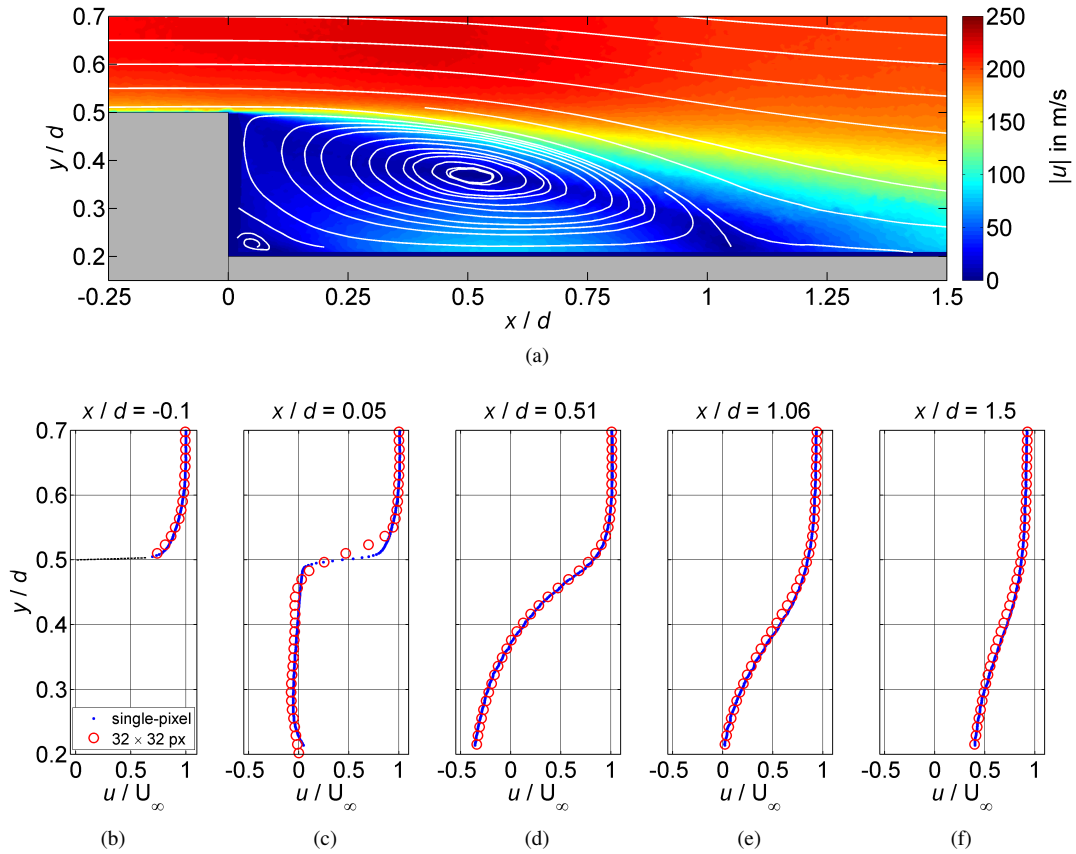


Figure 2: Mean velocity field and stream lines (a) of the generic space launcher model's wake flow ($Ma = 0.7$, $Re_d = 1.02 \times 10^6$) as well as profiles of the normalized horizontal mean velocity (b) at the end of the cylindrical forebody, (c) shortly after separation, (d) at the center of the primary recirculation region, (e) at reattachment and (f) after reattachment.

teristic profiles of the horizontal velocity component. The boundary layer upstream of the backward-facing step (figure 2b) strongly influences the wake flow topology (Bradshaw & Wong, 1972; Eaton & Johnston, 1981). The boundary layer thickness and the free stream velocity were estimated to be $\delta_{99} = (0.120 \pm 0.005)d = (6.5 \pm 0.3)$ mm and $U_\infty = (219.5 \pm 0.5)$ m s⁻¹, respectively. According to Bradshaw & Wong (1972), this backward-facing step can be considered as a strong perturbation, since the incoming boundary layer thickness is of the same order as the step height, which is $0.301 \cdot d$. The displacement thickness at $x/d = -0.1$ is $\delta_1/d > 0.0106$ and the momentum thickness is $\delta_2/d > 0.0091$ leading to a shape factor of $H_{12} = \delta_1/\delta_2 \approx 1.17$. Thus, for the analyzed Mach and Reynolds number combination the boundary layer at the end of the main body is fully turbulent, as desired.

Figure 2c shows the estimated profile of the horizontal velocity component in the shear layer shortly after separation at $x/d = 0.05$. The maximum shift vector gradient at $y/d = 0.5$ is larger than $\partial U/\partial Y = 0.5$ px px⁻¹ on the image plane (corresponding to $\partial u/\partial y \approx 1.7 \times 10^5$ s⁻¹). The strong change of the gradient in the radial direction could only be measured reliably with single-pixel ensemble-correlation. Window-correlation methods (red open circles) smear out the profile and underestimate the gradient, as discussed in detail in Kähler *et al.* (2012). The profile of the horizontal velocity component at the centre of the recirculation region is shown in figure 2d. It is characterized

by a large upstream component in the near wall region. The profile at the location of reattachment (figure 2e) shows a small gradient in the near-wall region and has a decreased horizontal velocity component in the outer region. Downstream of reattachment, the profile starts to develop into a turbulent boundary layer profile. The velocity profiles are in qualitative agreement with results presented in the literature (Scarano *et al.*, 1999; Deck & Thorigny, 2007; Schram *et al.*, 2004). But quantitatively there are significant differences: The experimental results based on window correlation evaluation methods results in reduced spatial resolution. As a result, the strong gradients in the incoming boundary layer as well as in the free shear layer are strongly underestimated by the other authors and therefore the results must be taken with care for the validation of numerical flow simulations and physical analysis.

REYNOLDS SHEAR STRESS DISTRIBUTION

As the reattachment of the flow is associated with the turbulent mixing in the shear layer, reliable measurements of the turbulent properties of the flow are of fundamental significance to predict the correct reattachment location by using numerical methods. The Reynolds shear stress $\langle u'v' \rangle$ is an indicator of the turbulence production in the xy -plane and is therefore an important parameter for the validation of modern numerical flow simulations as well as for physical interpretations of the flow.

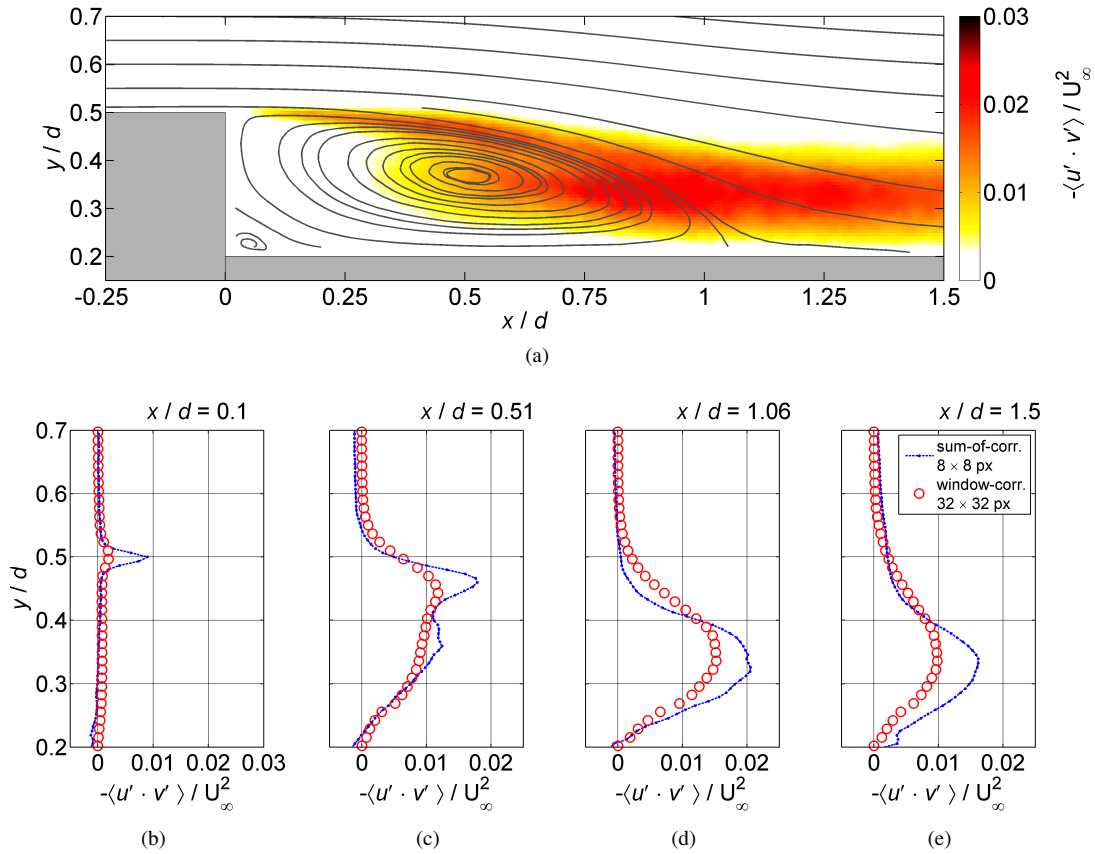


Figure 3: Reynolds shear stress distribution as well as profiles (b) shortly after separation, (c) at the center of the primary recirculation region, (d) at reattachment and (e) after reattachment.

Two approaches for the estimation of the Reynolds shear stress were applied: The first method computes in a classical way the shear stress from an ensemble of velocity fields:

$$\langle u'v' \rangle = \frac{1}{N} \sum_{n=1}^N (u_n - \langle u \rangle)(v_n - \langle v \rangle) \quad (1)$$

Where u and v are the axial and radial velocity components and N and n are the total number of vector fields and the corresponding control variable, respectively. Due to the fact that each vector represents the mean motion averaged over the interrogation-window size, the computed Reynolds stress values are spatially low-pass filtered, meaning that small turbulent structures (smaller than the interrogation-window size) are weighted lower than large ones.

To avoid these problems, a second method was developed which allows for the reliable estimation of Reynolds stresses without spatial low-pass filtering, by analysing the shape of ensemble averaged correlation functions. In this case, the whole ensemble of PIV image pairs is used to compute a map of correlation functions. The shape of each correlation function contains the information about the velocity's probability density function (*PDF*) of the in-plane velocity components (Adrian, 1988), from which the Reynolds stresses are computed as follows:

$$\langle u'v' \rangle = \int \text{PDF} u'v' du dv \quad (2)$$

The evaluation procedure was developed by the authors and is discussed in detail in Scharnowski *et al.* (2012).

Figure 3 shows the Reynolds shear stress distribution. While figure 3a illustrates only the results of the second method, figures 3b –3e compare results of the window-correlation (vector based) and sum-of-correlation (*PDF* based) approach.

A significant difference between the intensity of the estimated shear stress with the two methods is observed. Furthermore, the shape of the stress distribution differs: The window-correlation approach is not suited for the detection of the first part of the shear layer (see figure 3b), indicating that the shear stress here is dominated by small turbulent structures. The maximum position is around $x/d \approx 0.9$ in the case of window-correlation and around $x/d \approx 1.1$ for the sum-of-correlation approach, which includes the effect of small flow structures. The line plot at the center of the primary recirculation region in figure 3c shows two maxima in the case of sum-of-correlation function analysis, which correspond to the oscillating shear layer and to the breathing recirculation region. The stress estimation based on window-correlation cannot resolve this valley, which indicates the need for the approach applied here. It should also be noted that numerical simulations which are validated based on the classical PIV results would not be able to predict correct results as the physical model would be wrongly calibrated.

Figures 3c and 3d show a steep slope at the upper border of the shear layer for the sum-of-correlation approach, whereas this border is much smoother for the window-

August 28 - 30, 2013 Poitiers, France

correlation results. Additionally, the absolute value of the shear stress is larger in this region in the case of window-correlation. This fact indicates that the shear stress produced by larger vortices is partly cancelled by small ones.

CONCLUSIONS

Due to improved PIV evaluation methods it was possible to estimate turbulence statistics without spatial low-pass filtering at a Mach number of 0.7 and at a Reynolds number of 1.02×10^6 within the TWM facility. The mean flow field of the axisymmetric backward-facing step features a recirculation region that extends more than one model diameter in the axial direction. The shear layer reattaches on the model's rear sting at $x/d = 1.06$. The reattachment length is slightly shorter than predicted by numerical results at similar flow conditions (Deck & Thorigny, 2007). The motion of the separated shear layer causes an increase in the velocity fluctuations and thus in the Reynolds stress level. The combination of two approaches for estimating the Reynolds shear stresses revealed the contribution of turbulent structures with respect to their size. The use of both methods revealed the significance of small scale structures for the Reynolds stress distribution in the separated region. It was found that the first part of the shear layer is dominated by small structures, which cause significantly different shaped stress distributions. Furthermore, a distinct valley in the stress distributions was found between the shear layer and the primary recirculation region. Thus, it can be concluded that the application of sophisticated PIV evaluation methods is essential for the reliable estimation of flow statistics, such as the mean velocity field and the Reynolds stress distribution. In order to investigate the source of the differences between experimental results and numerical predictions it seems necessary to further increase the spatial resolution for the PIV experiments. Since the current resolution is limited by the vibration of the model

ACKNOWLEDGMENTS

Financial support from the German Research Foundation in the framework of the TRR 40 –Technological foundations for the design of thermally and mechanically highly loaded components of future space transportation systems– is gratefully acknowledged by the authors.

REFERENCES

- Adrian, R. J. 1988 Double Exposure, Multiple-Field Particle Image Velocimetry for Turbulent Probability Density. *Opt and Laser Eng* **9**, 211–228.
- Bitter, M., Hara, T., Hain, R., Yorita, D., Asai, K. & Kähler, C. J. 2012 Characterization of pressure dynamics in an axisymmetric separating/reattaching flow using fast-responding pressure-sensitive paint. *Exp Fluids* **53**, 1737–1749.
- Bitter, M., Scharnowski, S., Hain, R. & Kähler, C. J. 2011 High-repetition-rate PIV investigations on a generic rocket model in sub- and supersonic flows. *Exp Fluids* **50**, 1019–1030.
- Bradshaw, P. & Wong, F. Y. F. 1972 The reattachment and relaxation of a turbulent shear layer. *J Fluid Mech* **52**, 113–135.
- Chandrasuda, C. 1975 A reattaching turbulent shear layer in incompressible flow. PhD thesis, Imperial College London (University of London).
- Cierpka, C., Scharnowski, S. & Kähler, C.J. 2013 Parallax correction for precise near-wall flow investigations using particle imaging. *Applied Optics* **52**, 2923–2931.
- Deck, S. & Thorigny, P. 2007 Unsteadiness of an axisymmetric separating-reattaching flow: Numerical investigation. *Phys Fluids* **19**, 065103.
- Eaton, J. K. & Johnston, J. P. 1981 A Review of Research on Subsonic Turbulent Flow Reattachment. *AIAA Journal* **19**, 1093–1100.
- Kähler, C. J., Sammler, B. & Kompenhans, J. 2002 Generation and control of particle size distributions for optical velocity measurement techniques in fluid mechanics. *Exp Fluids* **33**, 736–742.
- Kähler, C. J., Scharnowski, S. & Cierpka, C. 2012 On the resolution limit of digital particle image velocimetry. *Exp Fluids* **52**, 1629–1639.
- Kähler, C. J., Scholz, U. & Ortmanns, J. 2006 Wall-shear-stress and near-wall turbulence measurements up to single pixel resolution by means of long-distance micro-PIV. *Exp Fluids* **41**, 327–341.
- McGuinness, M.D. 1978 Flow with a separation bubble: Steady and unsteady aspects. PhD thesis, University of Cambridge.
- Scarano, F., Benocci, C. & Riethmuller, M. L. 1999 Pattern recognition analysis of the turbulent flow past a backward facing step. *Phys Fluids* **11**, 3808.
- Scharnowski, S., Hain, R. & Kähler, C. J. 2012 Reynolds stress estimation up to single-pixel resolution using PIV-measurements. *Exp Fluids* **52**, 985–1002.
- Schram, C., Rambaud, P. & Riethmuller, M. L. 2004 Wavelet based eddy structure eduction from a backward facing step flow investigated using particle image velocimetry. *Exp Fluids* **36**, 233–245.
- Westerweel, J., Geelhoed, P. F. & Lindken, R. 2004 Single-pixel resolution ensemble correlation for micro-PIV applications. *Exp Fluids* **37**, 375–384.